DALTON
FULL PAPER

Cation distribution in cubic $NaM(PO_3)_3$ (M = Mg or Zn) using X-ray powder diffraction and solid state NMR †

Isaac Abrahams,*[a] Aliya Ahmed,[a] Christopher J. Groombridge,‡[a] Geoffrey E. Hawkes*[a] and Teresa G. Nunes[b]

[a] *Structural Chemistry Group, Department of Chemistry, Queen Mary and Westfield College, Mile End Road, London, UK E1 4NS. E-mail: I.Abrahams@qmw.ac.uk; G.E.Hawkes@qmw.ac.uk*
[b] *Instituto Superior Técnico, Departamento de Engenharia de Materiais, Av. Rovisco Pais, 1096 Lisboa Codex, Portugal*

Received 6th August 1999, Accepted 23rd November 1999

Solid state ^{23}Na and ^{31}P magic angle spinning nuclear magnetic resonance (MAS-NMR) spectroscopy and X-ray powder diffraction have been used in combination to study the structure of the model phosphate phases $NaMg(PO_3)_3$ and $NaZn(PO_3)_3$. The similar X-ray scattering of Na and Mg make determination of the cation distribution in $NaMg(PO_3)_3$ difficult using X-ray data alone. However, the structure of $NaZn(PO_3)_3$ was successfully refined and an initial model for the cation distribution in the magnesium analogue proposed. The ^{23}Na and ^{31}P solid state NMR data confirm the similarities between the two structures, while the ^{23}Na also suggested three sodium sites in a 2 : 1 : 1 ratio, consistent with the proposed crystallographic model. This allowed for a successful refinement of the structure of $NaMg(PO_3)_3$, confirming that the structures are indeed isostructural. Both structures contain chains of $(PO_3)_n^{n-}$ with Na^+ and Mg^{2+}/Zn^{2+} ions in distorted octahedral sites located between the polyphosphate chains.

There is considerable current interest[1] in the development of bioactive glasses and ceramics for medical use, as both bone and dental implants. A class of materials with particular promise is based on calcium phosphate, because of the chemical similarities with the apatitic nature of natural bone. Useful materials must exhibit both bioactivity and biocompatibility. Several groups[2–12] have recognised the potential of sodium/calcium/phosphate materials. Preliminary *in vitro* studies of a ternary Na_2O–CaO–P_2O_5 based system have shown a strong correlation between glass composition and cellular activity.[12,13] It has indicated that relatively low solubility glasses give greatly increased cellular activity and predictors of likely compositions to study have been drawn up. This work has indicated that low Na_2O (<28mol%) and low P_2O_5 (<45 mol%) promote cellular activity. We have also shown an upregulation in bone specific protein expression. Doping the materials with structure modifying oxides will change the bioactivity and biocompatibility, and a fundamental aim of our research is to seek correlations between such changes and modifications of short range structure. Therefore an important part of our programme is fully to characterise model phosphate phases which incorporate biologically relevant structure modifying oxides such as MgO and ZnO. To this end we have prepared and fully characterised the structures $NaMg(PO_3)_3$ and $NaZn(PO_3)_3$ using the synergy of the combination of solid state nuclear magnetic resonance and X-ray powder diffraction.

Experimental

Preparations

The phosphate compounds were synthesized by standard solid state methods. Appropriate stoichiometric amounts of Na_2CO_3 (BDH, 99%), $NH_4H_2PO_4$ (May & Baker, 97%) and ZnO (BDH, 99%) or MgO (BDH, 98%) were ground together as a slurry in ethanol. The dried mixture was placed in a platinum crucible and heated at 300 °C for 1 h to decompose the ammonium dihydrogenphosphate and subsequently further heated for 12 h at 650 °C before being quenched in air to room temperature. Phase purity was confirmed by X-ray powder diffraction.

Solid state NMR

The single-pulse ^{23}Na and ^{31}P NMR spectra were measured at 158.7 and 242.9 MHz respectively using a Bruker AMX-600 spectrometer. The samples were contained in a 4 mm o.d. rotor and magic angle spinning (MAS) was employed at 12 kHz. For each of the ^{23}Na spectra, 64 transients were accumulated, using a relaxation delay of 8 s, and a pulse width of $< \pi/20$, in order to be able to compare the intensities of resonances with differing quadrupole parameters.[14] The ^{23}Na chemical shifts were referenced to an external 1 M NaCl solution. For the ^{31}P spectra, MAS in the region 10 to 12 kHz was used and 50 to 100 transients were accumulated using a relaxation delay of 60 s. The ^{31}P chemical shifts were referenced to external 85% H_3PO_4. The two-dimensional triple-quantum ^{23}Na MAS spectra[15–17] were measured at 79.4 MHz using a Bruker MSL-300 spectrometer. The samples were contained in a 4 mm o.d. rotor and MAS used at 10 kHz; 96 transients were accumulated with a 10 s recycle time; 512 and 256 points were acquired in the F1 and F2 dimensions respectively. The ^{23}Na MAS NMR spectra were simulated using the program QUASAR.[18] The intensities of the spinning sideband groups in the ^{31}P MAS NMR spectra were determined using the Bruker 1-D WINNMR PC software, and the ^{31}P shielding tensor components were determined from these line intensities with the Bruker WINMAS program.[19]

X-Ray crystallography

X-Ray powder diffraction data were collected on both compounds using an automated Philips PW1050/30 diffractometer. Data were collected using Ni filtered Cu-Kα radiation

† Dedicated to Professor Donald C. Bradley FRS on the occasion of his 75th birthday.
‡ Present address: The Forensic Science Service, 109 Lambeth Road, London, UK SE1 7LP.

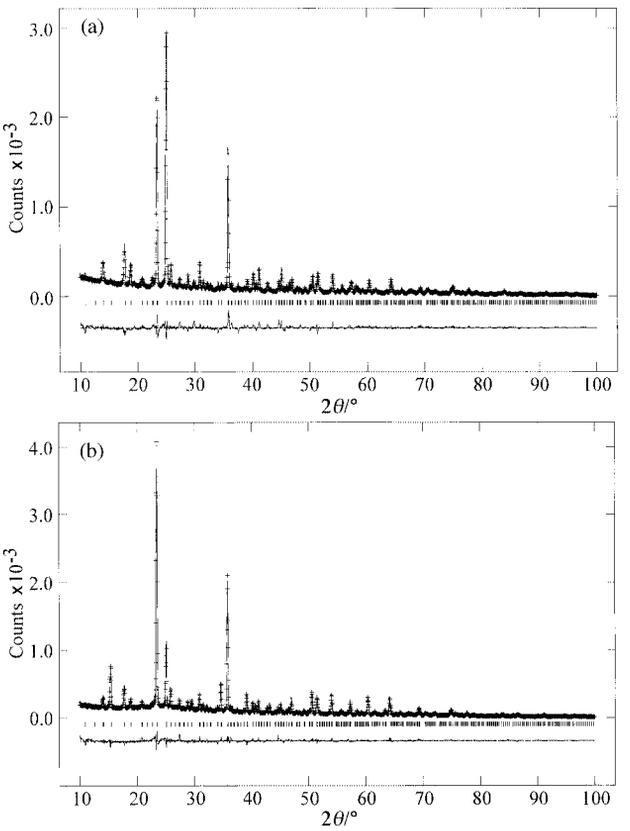

Fig. 1 Fitted diffraction profiles for (a) $NaMg(PO_3)_3$ and (b) $NaZn(PO_3)_3$ showing observed (+ signs), calculated (line) and difference (lower) profiles. Reflection positions are indicated by markers.

($\lambda = 1.5418$ Å) in flat plate θ–2θ geometry in the range 5–110° 2θ, in steps of 0.02°, with a count time of 10 s per step. A flat plate absorption correction was applied prior to refinement. The structure refinement was carried out by the Rietveld method, using the GSAS suite of programs.[20] Refinement of an initial model based on the published[21] orthorhombic structure of $NaMg(PO_3)_3$ ($a = 14.304$, $b = 14.183$, $c = 14.231$ Å, space group *Pbca*, no. 61[22]) suggested that both structures were actually of cubic symmetry with $a \approx 14.23$ Å for Mg and 14.24 Å for Zn. There was no evidence of a splitting of the cubic reflections consistent with an orthorhombic distortion. This is consistent with the cubic cell parameters reported for $NaZn(PO_3)_3$ by Averbuch-Pouchot *et al.*[23] Systematic absences suggested $Pa\bar{3}$ (no. 205)[22] as a possible space group. The structure of orthorhombic[21] $NaMg(PO_3)_3$ was used to generate an initial model, with cations distributed over five crystallographically distinct sites. In order to determine the correct cation distribution the Zn containing system was refined first. The relatively large difference in X-ray scattering between Zn and Na meant that the correct cation distribution was more readily refined from this system than the Mg containing compound, Mg having very similar X-ray scattering to Na. The ^{23}Na solid state NMR indicated three sodium sites in an approximate 2 : 1 : 1 ratio in both compounds. Therefore the sodium were identified as two 4-fold sites and an 8-fold site. Refinements on other combinations of Na/Zn sites generally resulted in higher R factors. The final structural parameters for $NaZn(PO_3)_3$ were used to generate an initial model for the magnesium analogue, which subsequently refined satisfactorily. In both, isotropic thermal parameters were refined for all atoms with those for like atoms tied to each other, apart from Zn(1) and Zn(2). Soft constraints were applied to the P–O distances, with bridging and terminal bonds constrained close to the values observed in the orthorhombic form of $NaMg(PO_3)_3$. Crystal parameters are summarised in Table 3. The final refined parameters are shown in Table 4 with

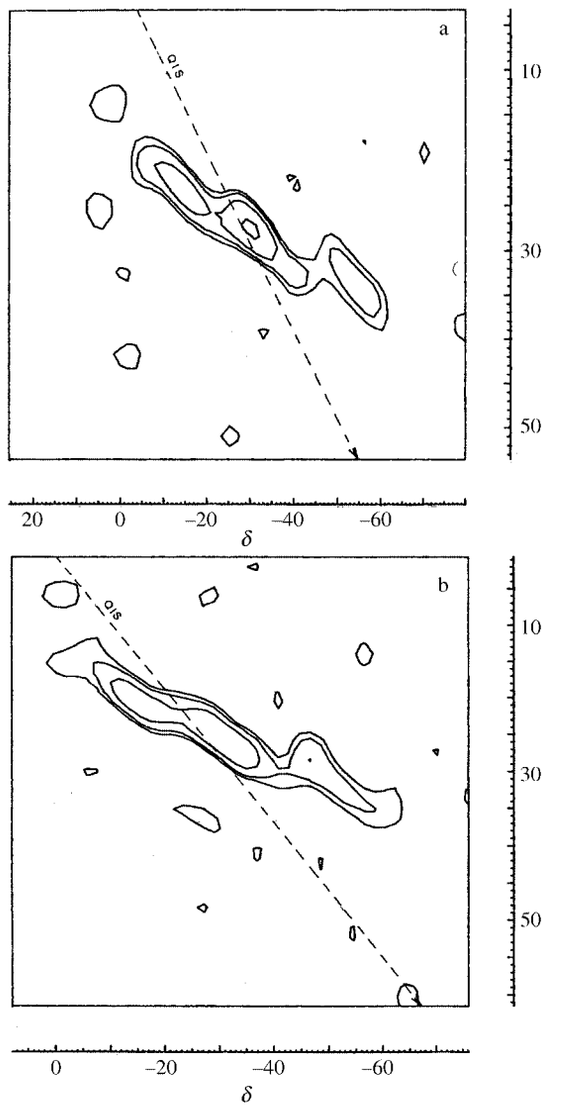

Fig. 2 The 79.4 MHz ^{23}Na triple quantum 2-D NMR spectra of (a) $NaMg(PO_3)_3$ and (b) $NaZn(PO_3)_3$. Each spectrum clearly shows three principal sodium sites. The dotted lines labelled QIS are the 'quadrupole induced shift' axes.

significant contact distances and angles in Table 5. The corresponding fitted diffraction profiles are shown in Fig. 1.

Results and discussion

^{23}Na NMR spectra

The solid state single pulse ^{23}Na MAS spectra of $NaMg(PO_3)_3$ and $NaZn(PO_3)_3$ are quite similar to each other, both consisting of a single broad signal with a number of superimposed sharp features. It is clear that the spectra are the result of two or more overlapping sodium resonances and the two-dimensional triple-quantum spectra[15–17] were measured in order to determine the number of overlapping resonances in each spectrum. The results are shown in Fig. 2, and it is seen that there are three principal sodium resonances contributing to each spectrum. The additional information from each spectrum are the isotropic chemical shifts and the 'second order quadrupole' parameters[16] (SOQE), eqn. (1), where C_q and η_q are the quad-

$$\mathrm{SOQE} = C_q\left(1 + \frac{\eta_q^2}{3}\right)^{1/2} \quad (1)$$

rupole coupling constant and asymmetry parameter respectively. The SOQE values obtained are given in Table 1. The values for the quadrupole parameters and isotropic shifts

Table 1 Parameters from the analysis of the ^{23}Na MAS NMR spectra

	Site	Population (%)	C_q/MHz	η_q	δ_{iso} [a]
$NaMg(PO_3)_3$	1	43 ± 4	2.67 ± 0.03	0.34 ± 0.06	0.0
	2	26 ± 1	2.57 ± 0.04	0.47 ± 0.04	−4.3
	3	31 ± 1	2.72 ± 0.02	0.59 ± 0.02	−9.8
$NaZn(PO_3)_3$	1	41 ± 2	2.50 ± 0.04	0.38 ± 0.03	0.0
	2	28 ± 2	2.66 ± 0.02	0.51 ± 0.02	−4.1
	3	31 ± 1	2.67 ± 0.05	0.59 ± 0.04	−9.9

[a] Value in ppm.

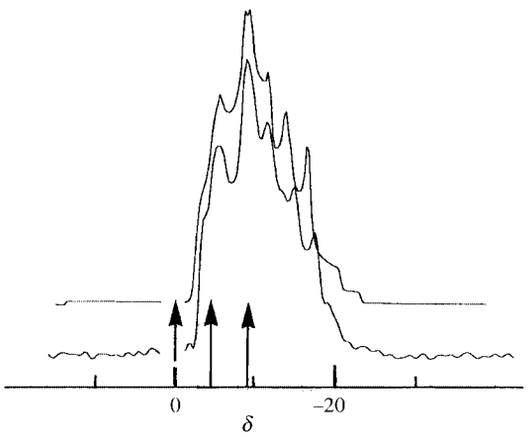

Fig. 3 158.7 MHz single-pulse ^{23}Na MAS NMR spectrum of $NaMg(PO_3)_3$. The lower spectrum is the experimental and the upper is calculated using the best fit parameters given in Table 1. Vertical arrows indicate the isotropic chemical shifts.

were refined by iterative simulation of the single pulse ^{23}Na MAS spectra and the values obtained are also given in Table 1 (see also Fig. 3). It is obvious from the data that the sodium environments in the two samples are very similar, each displaying three principal sites with similar isotropic shifts, quadrupole coupling constants and asymmetry parameters. The site occupancy ratios for the three sodium sites in each structure are close to 2 : 1 : 1, and this information was valuable input to the modelling of the X-ray data (vide infra). From consideration of the populations, the sodium in site 1 (Table 1) corresponds to Na(3) in the crystallographic analysis (Tables 4 and 5). The isotropic ^{23}Na chemical shifts are very similar to those we reported[10] for ^{23}Na in a series of Na/Ca/phosphate glass ceramics (δ 5.7 to −13.4). The quadrupole coupling constants (C_q) determined here fall within a relatively narrow range (2.50 to 2.72 MHz) and are measurably larger than those found for the glass ceramics[10] (1.41 to 2.36 MHz) and for some simple sodium ortho- and meta-phosphates[24] (1.19 to 2.20 MHz). It is noteworthy that for both NaMg and NaZn phases the values for the asymmetry parameters vary in the same way, *i.e.* site 3 > site 2 > site 1, although we do not believe it is possible to use this observation to assist in the assignment of NMR sites 2 and 3 to crystallographic sites Na(1) and Na(2).

^{31}P NMR spectra

The solid state ^{31}P MAS NMR spectra of $NaMg(PO_3)_3$ and $NaZn(PO_3)_3$ are shown in Fig. 4. For the NaZn phase there are four more or less well resolved lines at δ −28.3, −30.0, −31.1 and −32.5, whereas for the NaMg phase there is a more complicated pattern in the same spectral region. This chemical shift region is within the range quoted by Haubenreisser *et al.*[25] for metaphosphate Q^2 units in polycrystalline phosphates δ −18 to −53. The X-ray crystallography (see below) shows for both phases there are two distinct phosphorus sites which alternate along the metaphosphate chains. If we designate these two sites as A and B, and consider finite two bond homonuclear ^{31}P–^{31}P scalar coupling between adjacent PO_3 groups (measured[26–28] in

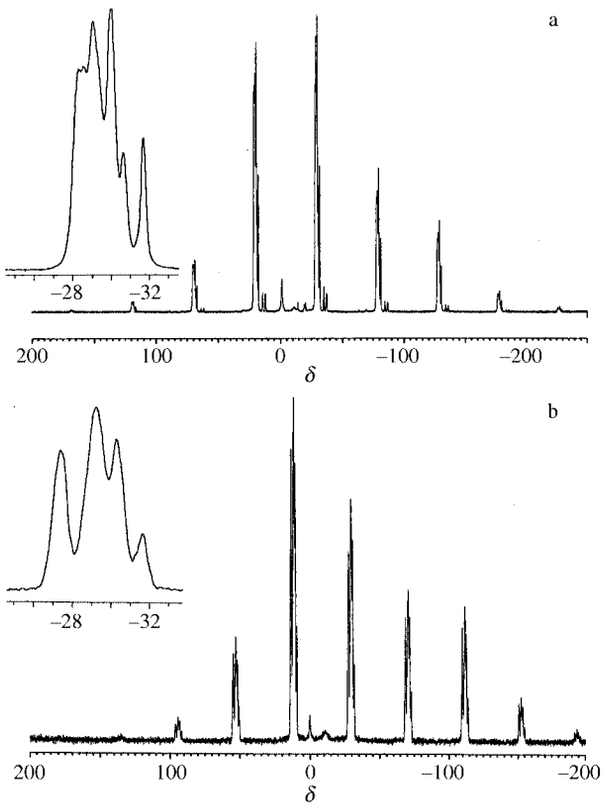

Fig. 4 The 242.9 MHz ^{31}P MAS NMR spectra of (a) $NaMg(PO_3)_3$, 89 transients accumulated with the MAS rate = 12 kHz, and (b) $NaZn(PO_3)_3$, 50 transients accumulated with the MAS rate = 10 kHz. Inset to each spectrum is the expansion of the centre band region.

the range 17 to 20 Hz) then the spin system may be designated as $[AB]_n$ or $[AX]_n$, depending upon the relative magnitudes of the scalar coupling and the chemical shift separation. The MAS spectra of spin $\frac{1}{2}$ nuclei in the presence of homonuclear scalar and dipolar coupling may be complicated through the appearance of additional lines in the spectra, as well as line broadening.[28–30] Dusold *et al.*[28,31] have simulated experimental MAS spectra for an AA′ spin pair and a three spin ABX system. The AA′ ^{31}P system of $Na_4P_2O_7{\cdot}10H_2O$ has a single isotropic ^{31}P chemical shift, ^{31}P–^{31}P scalar coupling *ca.* 20 Hz, and a ^{31}P–^{31}P dipolar coupling of 791 Hz. There are clearly splittings in the reported spectra which are >200 Hz and which are not due to chemical shift differences, nor directly to ^{31}P–^{31}P scalar coupling. Instead the ^{31}P–^{31}P dipolar coupling and the orientations of the chemical shift and dipolar tensors are important. To the best of our knowledge there have been no simulations on the $[AB]_n$ or $[AX]_n$ system seen here, but, since both scalar and dipolar couplings in these metaphosphate chains must be very similar to those in the $P_2O_7^{4-}$ case,[28] it is safe to assume that the same mechanism is operative, causing the more complicated appearance of the ^{31}P spectra.

The isotropic ^{31}P chemical shift ranges for the two phases are quite similar at δ −28 to −33 for NaZn and −28 to −32 for NaMg, and these ranges are significantly to lower frequency

than we reported [10–12] (δ −18 to −25) for Q^2 phosphorus in the Na/Ca/phosphate glass ceramics. However, in those ceramics the Q^2 phosphorus was believed to be present as discrete cyclic trimetaphosphate rings and so the ^{31}P isotropic shifts may not be comparable to those from the metaphosphate chains in this study. Turner *et al.*[32] measured the solid state ^{31}P isotropic chemical shifts for a series of metal orthophosphates and obtained a good empirical correlation between the shift and the ionic radius of the metal (r), eqn. (2). If a similar correlation

$$\delta_{iso} = -7.7r^{-\frac{1}{2}} + 18.6 \quad (2)$$

holds for structurally similar metaphosphates, then the near identical ionic radii [33] for 6-co-ordinate Mg^{2+} (0.72 Å) and Zn^{2+} (0.75 Å) should give very similar ^{31}P chemical shifts, as seen in the present study.

The full ^{31}P spectrum for $NaMg(PO_3)_3$ showed additional minor signals for which the intensity varied with sample preparation, and these were therefore assigned to minor impurities: δ −1, orthophosphate (Q^0); −10 to −20, pyrophosphate (Q^1) (end groups of the metaphosphate chains may also contribute); −36, −38 possibly metaphosphate (Q^2). Apart from a small orthophosphate ^{31}P signal around δ −1 and a Q^1 residue around δ −10, the preparations of $NaZn(PO_3)_3$ were essentially free from impurities. In both cases no evidence of significant crystalline impurities was observed in the X-ray powder diffraction data.

The intensities of the spinning sideband manifold may be used to calculate values for the individual components of the ^{31}P nuclear shielding tensor. Since we are unable to assign specific lines within each sideband to the distinct phosphorus sites, the total integrated intensity of each sideband was determined and used to calculate an average for the shielding tensor components. The analysis of the side band intensities used the method of Herzfeld and Berger [34] (see Experimental section) and yields the principal components (δ_{11}, δ_{22}, δ_{33}) of the chemical shift tensor, for which the isotropic chemical shift (δ_{iso}) is given by eqn. (3). These principal elements were ordered

$$\delta_{iso} = (\delta_{11} + \delta_{22} + \delta_{33})/3 \quad (3)$$

according to the Haeberlen convention: [35] $|\delta_{33} - \delta_{iso}| > |\delta_{11} - \delta_{iso}| > |\delta_{22} - \delta_{iso}|$. The chemical shift anisotropy ($\Delta\delta$) and asymmetry parameter (η) are given by eqns. (4) and (5). The

$$\Delta\delta = \delta_{33} - (\delta_{11} + \delta_{22})/2 \quad (4)$$

$$\eta = (\delta_{22} - \delta_{11})/(\delta_{33} - \delta_{iso}) \quad (5)$$

results of the shielding tensor analysis are given in Table 2. The most important parameter is the chemical shift anisotropy ($\Delta\delta$) which is very similar for the two phosphate phases, around −200 ppm. This is within the range (−160 to −250 ppm) quoted by Haubenreisser *et al.*[25] and close to the values reported by us [10] for the Na/Ca/phosphate glass ceramics. The shift anisotropy is a particularly useful parameter in determining whether a ^{31}P isotropic shift is due to Q^2 or to Q^1 phosphorus. According to Haubenreisser *et al.*[25] the isotropic shift ranges do overlap with Q^1 at δ +4 to −33 and Q^2 at δ −18 to −53, but with quoted [25] ranges for $\Delta\delta$ from Q^1 units as 14 to 80 ppm and for Q^2 units −160 to −250 ppm, there is no ambiguity.

X-Ray crystallography

The compounds $NaMg(PO_3)_3$ and $NaZn(PO_3)_3$ are isostructural. A projection of the unit cell contents is shown in Fig. 5. The structures are built from polyphosphate chains $(PO_3)_n^{n-}$, with Na^+ and Mg^{2+} or Zn^{2+} ions located in distorted octahedral cavities between the chains. The polyphosphate chains consist of apex sharing PO_4 tetrahedra, with two shared and two terminal oxygen atoms in each tetrahedron. Two crystallographically distinct phosphorus sites are observed. The sodium ions are co-ordinated to six terminal phosphate oxygen atoms with three crystallographically distinct sodium found. Similarly the Mg^{2+}/Zn^{2+} ions are co-ordinated to six terminal phosphate oxygens, over two crystallographically distinct sites.

Atoms Na(1) and Na(2) have similar co-ordinations to the phosphate chains; Na(1) is co-ordinated to six terminal O(3) atoms on the polyphosphate chains in a distorted octahedral environment, at a distance of 2.38 Å for both structures. Similarly Na(2) is also located in a distorted octahedral site and is

Table 2 ^{31}P Anisotropic chemical shift data for $NaMg(PO_3)_3$ and $NaZn(PO_3)_3$

	$NaMg(PO_3)_3$	$NaZn(PO_3)_3$
δ_{11} [a]	66.0 ± 0.5	63.1 ± 3.9
δ_{22} [a]	9.2 ± 0.4	10.4 ± 3.8
δ_{33} [a]	−162.8 ± 0.4	−161.3 ± 0.3
$\Delta\delta$ [a]	−200.4	−198.1
η	0.43	0.40

[a] Values in ppm.

Table 3 Crystal parameters for $NaMg(PO_3)_3$ and $NaZn(PO_3)_3$

Empirical formula	$MgNaO_9P_3$	NaO_9P_3Zn
Formula weight	284.22	325.28
Crystal system	Cubic	Cubic
Space group	$Pa\bar{3}$	$Pa\bar{3}$
Z	16	16
μ/mm^{-1}	9.60	12.24
$F(000)$	2240	2528
a/Å	14.2502(6)	14.2581(4)
V/Å^3	2893.7(4)	2898.6(3)
D_c/g cm^{-3}	2.610	2.983
R_{wp},R_p [a]	0.1286, 0.0981	0.0997, 0.0760
R_{ex}	0.1015	0.0951
R_F^2	0.1512	0.1425
χ^2	1.631	1.422
No. of reflections	1018	1018
2θ range collected/°	5–115	5–115
Step width/°	0.02	0.02
2θ range refined/°	10.–100	10–100
Observations/restraints/parameters	4499/8/50	4499/8/51
Maximum atomic shift/Å	0.09	0.03

[a] For definition of R factors see ref. 36.

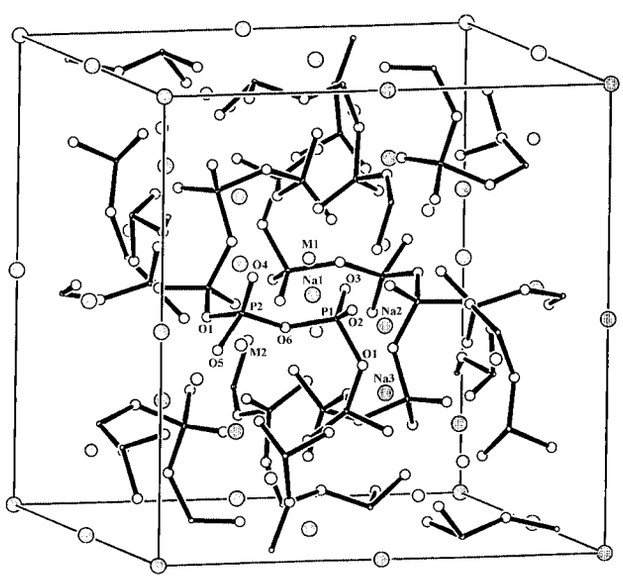

Fig. 5 Unit cell projection of $NaM(PO_3)_3$ (M = Mg or Zn), showing P (small open circles), O (large open circles), Mg/Zn (small shaded circles) and Na (large shaded circles) atoms.[37]

Table 4 Refined atomic parameters for (a) $NaMg(PO_3)_3$ and (b) $NaZn(PO_3)_3$ with estimated standard deviations in parentheses

Atom	Wyckoff site	*x*	*y*	*z*	U_{iso}/Å^2
(a)					
Na(1)	4*b*	0.5(−)	0.5(−)	0.5(−)	0.026(2)
Na(2)	4*a*	0.0(−)	0.0(−)	0.0(−)	0.026(2)
Na(3)	8*c*	0.2445(5)	0.2445(5)	0.2445(5)	0.026(2)
Mg(1)	8*c*	0.1269(7)	0.1269(7)	0.1269(7)	0.012(2)
Mg(2)	8*c*	0.3846(6)	0.3846(6)	0.3846(6)	0.012(2)
P(1)	24*d*	0.0247(4)	0.2386(4)	0.4850(4)	0.021(3)
P(2)	24*d*	0.2308(4)	0.2199(5)	0.4986(5)	0.038(3)
O(1)	24*d*	0.4832(5)	0.2676(7)	0.1151(5)	0.018(1)
O(2)	24*d*	0.0273(11)	0.1605(5)	0.0102(10)	0.018(1)
O(3)	24*d*	0.4729(8)	0.3386(7)	0.4681(9)	0.018(1)
O(4)	24*d*	0.2203(10)	0.2135(8)	0.0778(6)	0.018(1)
O(5)	24*d*	0.2843(9)	0.2591(9)	0.4186(7)	0.018(1)
O(6)	24*d*	0.1259(4)	0.1922(7)	0.4691(9)	0.018(1)
(b)					
Na(1)	4*b*	0.5(−)	0.5(−)	0.5(−)	0.035(3)
Na(2)	4*a*	0.0(−)	0.0(−)	0.0(−)	0.035(3)
Na(3)	8*c*	0.2486(7)	0.2486(7)	0.2486(7)	0.035(3)
Zn(1)	8*c*	0.1300(5)	0.1300(5)	0.1300(5)	0.011(2)
Zn(2)	8*c*	0.3807(5)	0.3807(5)	0.3807(5)	0.051(3)
P(1)	24*d*	0.0236(6)	0.2410(5)	0.4814(6)	0.028(3)
P(2)	24*d*	0.2279(6)	0.2180(5)	0.4952(6)	0.046(4)
O(1)	24*d*	0.4750(7)	0.2728(10)	0.1146(8)	0.027(2)
O(2)	24*d*	0.0222(13)	0.1600(6)	0.0127(13)	0.027(2)
O(3)	24*d*	0.4803(12)	0.3377(9)	0.4665(11)	0.027(2)
O(4)	24*d*	0.2248(14)	0.2221(13)	0.0799(8)	0.027(2)
O(5)	24*d*	0.2934(11)	0.2533(11)	0.4228(9)	0.027(2)
O(6)	24*d*	0.1239(7)	0.1955(13)	0.4594(14)	0.027(2)

Table 5 Significant bond lengths and contact distances (Å) in $NaM(PO_3)_3$ (M = Mg or Zn) with estimated standard deviations in parentheses

	$NaMg(PO_3)_3$	$NaZn(PO_3)_3$
Na(1)–O(3)	2.377(10) × 6	2.379(13) × 3
Na(2)–O(2)	2.325(7) × 6	2.311(9) × 6
Na(3)–O(4)	2.441(11) × 3	2.458(15) × 3
Na(3)–O(5)	2.552(13) × 3	2.566(17) × 3
Mg(1)–O(2)	2.238(18) × 3	2.311(20) × 3
Mg(1)–O(4)	1.945(16) × 3	2.016(19) × 3
Mg(2)–O(3)	1.852(15) × 3	1.973(17) × 3
Mg(2)–O(5)	2.339(15) × 3	2.282(17) × 3
P(1)–O(1)	1.599(10)	1.600(14)
P(1)–O(2)	1.482(9)	1.480(12)
P(1)–O(3)	1.483(13)	1.480(16)
P(1)–O(6)	1.602(9)	1.601(15)
P(2)–O(1)	1.597(10)	1.632(15)
P(2)–O(4)	1.483(12)	1.481(16)
P(2)–O(5)	1.482(13)	1.480(17)
P(2)–O(6)	1.603(9)	1.601(14)

linked to six terminal O(2) atoms on the polyphosphate chains at distances of 2.33 and 2.31 Å for Mg and Zn structures respectively. A distorted octahedral site is also seen for Na(3) with three contacts to O(4) at 2.44 and 2.46 Å and three to O(5) at 2.55 and 2.57 Å for Mg and Zn structures respectively. The site geometries are similar to those observed in orthorhombic $NaMg(PO_3)_3$, which showed Na–O distances ranging from 2.338 to 2.559 Å.[21]

The Zn/Mg octahedral sites are heavily distorted. Each site shows three short Zn/Mg–O contacts and three longer contacts with distances ranging from 1.85–2.34 and 1.97–2.31 Å for Mg–O and Zn–O respectively. This contrasts with the orthorhombic form of $NaMg(PO_3)_3$, which showed more regular oxygen coordination environments for Mg, with distances ranging from 2.018 to 2.143 Å. In the $NaZn(PO_3)_3$ structure the Zn(1) and Zn(2) isotropic thermal parameters were allowed to refine independently of each other. The refined Zn(1) isotropic parameter is significantly lower, at 0.011 Å^2, than that for Zn(2), at 0.051 Å^2. While both of these values are within acceptable limits for this type of structure, the observed difference may reflect greater positional/thermal disorder on the Zn(2) site, or indeed be due to a small amount of substitution by Na on this site. A low level of a fourth sodium site would be undetectable in the NMR spectrum.

If we compare the observed crystal structure for $NaMg(PO_3)_3$ with that previously reported[21] in orthorhombic symmetry, we can see that the six crystallographically unique phosphorus sites in the orthorhombic structure are averaged to two unique sites in the present cubic phase. It is possible that the NMR evidence suggests more than two phosphorus environments, and in this case the observed phosphorus positions represent averages, and that a number of local coordinations may exist but are disordered over the lattice resulting in the observed average cubic structure. These results confirm the usefulness of the parallel ^{31}P MAS NMR study which is more sensitive to small variations in local coordination than is the X-ray powder crystallographic technique.

Conclusion

The present study illustrates the value of combined approaches to structure determination. From the X-ray data alone it would have been difficult to determine the true cation distribution in $NaMg(PO_3)_3$, due to the similar X-ray scattering of Na and Mg. However, the fact that the zinc analogue is isostructural and could be refined satisfactorily allowed for an initial model to be proposed for the cation distribution in the magnesium structure. The ^{31}P and ^{23}Na NMR data confirm the similarities of the two structures. In addition the ^{23}Na data suggest a likely Na^+ ion distribution which is consistent between the two structures. Hence the cation distribution in sodium magnesium phosphate was determined. The question of the number of lines in the ^{31}P MAS NMR spectrum being greater than that predicted from the crystallography remains unsolved. Prabhakar *et al.*,[38] in an important earlier study, reported that the number of observed ^{31}P MAS NMR signals from meta- and pyro-phosphates could outnumber the crystallographically

distinguishable phosphorus sites. There are two possible explanations. The first is that the ^{31}P chemical shifts are sensitive to local variations in co-ordination whereas the crystallography is giving an average over long range order in the solid. The second is that the combination of the NMR parameters, scalar and dipolar coupling, and the orientations of the chemical shift and dipolar tensors is producing more complex spectra. Both effects may operate in parallel and this aspect is the subject of continuing investigation.

Acknowledgements

Two of us (T. G. N. and I. A.) thank NATO for a Collaborative Research Grant. We thank the University of London Intercollegiate Research Service in High Field NMR at Queen Mary and Westfield College for the provision of the Bruker AMX-600 NMR spectrometer.

References

1 W. Vogel and W. Höland, *Angew. Chem., Int. Ed. Engl.*, 1987, **26**, 527.
2 R. K. Brow, R. J. Kirkpatrick and G. L. Turner, *J. Non-Cryst. Solids*, 1990, **116**, 39.
3 R. K. Brow, D. R. Tallant, J. J. Hudgens, S. W. Martin and A. D. Irwin, *J. Non-Cryst. Solids*, 1994, **177**, 221.
4 J. P. Fletcher, R. J. Kirkpatrick, D. Howell and S. H. Rishbud, *J. Chem. Soc., Faraday Trans.*, 1993, 3297.
5 R. J. Kirkpatrick and R. K. Brow, *Solid State NMR*, 1995, **5**, 9.
6 P. Hartmann, J. Vogel and B. Schnabel, *J. Non-Cryst. Solids*, 1994, **176**, 157.
7 C. Jáger, P. Hartmann, G. Kunath-Fandrei, O. Hirsch, P. Rehak, J. Vogel, M. Feike, H. W. Spiess, K. Herzog and B. Thomas, *Ber. Bunsenges. Phys. Chem.*, 1996, **100**, 1560.
8 P. Hartmann, J. Vogel and C. Jáger, *Ber. Bunsenges. Phys. Chem.*, 1996, **100**, 1658.
9 R. Witter, P. Hartmann, J. Vogel and C. Jáger, *Solid State NMR*, 1998, **13**, 189.
10 I. Abrahams, K. Franks, G. E. Hawkes, G. Philippou, J. Knowles, P. Bodart and T. Nunes, *J. Mater. Chem.*, 1997, **7**, 1573.
11 I. Abrahams, G. E. Hawkes and J. Knowles, *J. Chem. Soc., Dalton Trans.*, 1997, 1483.
12 K. Franks, J. C. Knowles, G. E. Hawkes, I. Abrahams, I. Jalisi and D. Lee, *J. Dent. Res.*, 1998, **77**, 1047.
13 V. Salih, K. Franks, M. James, G. W. Hastings, J. C. Knowles and I. Olsen, *J. Dent. Res.*, 1999, **78**, 1075.
14 D. Fenzke, D. Freude, T. Fröhlich and J. Haase, *Chem. Phys. Lett.*, 1984, **111**, 171.
15 L. Frydman and J. S. Harwood, *J. Am. Chem. Soc.*, 1995, **117**, 5367.
16 C. Fernandez and J. P. Amoureux, *Chem. Phys. Lett.*, 1995, **242**, 449.
17 C. Fernandez and J. P. Amoureux, *Solid State NMR*, 1996, **6**, 315.
18 J. P. Amoureux, C. Fernandez, L. Carpentier and E. Cochon, *Phys. Status Solidi. A*, 1992, **132**, 461.
19 WINMAS, version 951208, Bruker-Franzen Analytik GmbH, Bremen, 1995.
20 A. C. Larson, R. B. Von Dreele and M. Lujan, Jr., GSAS. Generalised Structural Analysis System, Neutron Scattering Centre, Los Alamos National Laboratory, CA, 1990.
21 Y. F. Shepelev, Yu. I. Smolin, A. I. Domanskii and A. V. Lavarov, *Dokl. Akad. Nauk SSSR*, 1983, **272**, 610.
22 *International Tables for Crystallography*, ed. T. Hahn, IUCR, Kluwer Academic Publishers, Dordrecht, 1992, vol. A.
23 M-T. Averbuch-Pouchot, E. Rakotomahanina-Rolaisoa and A. Durif, *Bull. Soc. Fr. Miner. Cristallogr.*, 1970, **93**, 282.
24 H. Koller, G. Engelhardt, A. P. M. Kentgens and J. Sauer, *J. Phys. Chem.*, 1994, **98**, 1544.
25 H. Haubenreisser, J. Vogel, W. Höland and W. Vogel, *Wiss. Zt. Friedrich-Schiller-Univ. Jena,* Math.-Naturwiss. Reihe, 1987, **36**, 763.
26 M. M. Crutchfield, C. F. Callis, R. R. Irani and G. C. Roth, *Inorg. Chem.*, 1962, **1**, 813.
27 M. Cohn and T. R. Hughes, *J. Biol. Chem.*, 1960, **235**, 3250.
28 S. Dusold, W. Milius and A. Sebald, *J. Magn. Reson.*, 1998, **135**, 500.
29 T. Nakai and C. A. McDowell, *Mol. Phys.*, 1992, **77**, 569.
30 G. Wu, B. Q. Sun, R. E. Wasylishen and R. G. Griffin, *J. Magn. Reson.*, 1997, **124**, 366.
31 S. Dusold and A. Sebald, *Mol. Phys.*, 1998, **95**, 1237.
32 G. L. Turner, K. A. Smith, R. J. Kirkpatrick and E. Oldfield, *J. Magn. Reson.*, 1986, **70**, 408.
33 R. D. Shannon and C. T. Prewitt, *Acta Crystallogr., Sect. B*, 1969, **25**, 925; 1970, **26**, 1046.
34 J. Herzfeld and A. E. Berger, *J. Chem. Phys.*, 1980, **73**, 6021.
35 U. Haeberlen, *High Resolution NMR in Solids - Selective Averaging*, Academic Press, New York, 1976, p. 9.
36 *The Rietveld Method*, ed. R. A. Young, IUCR monographs on Crystallography 5, Oxford University Press, New York, 1993, p. 21.
37 L. J. Farrugia, *J. Appl. Crystallogr.*, 1997, **30**, 565.
38 S. Prabhakar, K. J. Rao and C. N. R. Rao, *Chem. Phys. Lett.*, 1987, **139**, 96.

Paper a906413c